Supporting Information

Low Cost & Quasi Solid State $Na_2Mn_{0.5}Ni_{0.5}Fe(CN)_6$//$Na_xFe_2O_3$ Hybrid Na-Ion Batteries for Solar Energy Storage

Pappu Naskar[a], Shubhrajyoti Mondal[a], Biplab Biswas[a], Sourav Laha[b*] and Anjan Banerjee[a*]

[a] Department of Chemistry, Presidency University-Kolkata, Kolkata-700073, India

[b] Department of Chemistry, National Institute of Technology Durgapur, Durgapur-713209, India

Supporting Tables

Table S1. Calculation of Na-ion diffusion coefficient for Mn-PBA and MnNi-PBA.

Parameter / Unit	Mn-PBA	MnNi-PBA
R (J K^{-1} mol^{-1})	8.314	8.314
T (K)	303	303
A (cm^2)	1	1
n	2	1.5
F (Coulomb mol^{-1})	96485	96485
#C (mol cm^{-3})	0.0114	0.017
σ (Ohm $s^{-0.5}$)	180	**77**
D (cm^2 s^{-1})	5.4×10^{-16}	4.2×10^{-15}

#C value is calculated from the crystal structures of the active materials, which are established by Rietveld refinement of PXRD data.

For Mn-PBA

Formula unit per unit cell (Z) = 2

Unit cell volume = 582.563 $Å^3$

Hence, 4 Na^+ ion present in 582.563 $Å^3$

Therefore, 0.0114 mole Na^+ ion present in 1 cm^{-3}

For MnNi-PBA

Formula unit per unit cell (Z) = 2

Unit cell volume = 563.716 $Å^3$

Hence, 4 Na^+ ion present in 563.716$Å^3$

Therefore, 0.017 mole Na^+ ion present in 1 cm^{-3}

Table S2. Structural parameters and atomic positions obtained from Rietveld refinement of PXRD data on Mn-PBA.

Atom	**site**	**x**	**y**	**z**	**U_{iso}**	**Occupancy**
Mn	2a	0.5	0.5	0.5	0.004(4)	1.0
Fe	2d	0.5	0	1.0	0.024(5)	0.99(2)
Na	4e	0.240(4)	0.481(10)	0.051(9)	0.066(9)	0.93(1)
N	4e	0.544(4)	0.286(7)	0.811(6)	0.034(6)	1.0
N	4e	0.285(4)	0.574(6)	0.484(6)	0.034(6)	1.0
N	4e	0.505(6)	0.266(7)	0.306(5)	0.034(6)	1.0
C	4e	0.524(6)	0.181(7)	0.847(7)	0.034(6)	1.0
C	4e	0.188(4)	0.491(10)	0.530(6)	0.034(6)	1.0
C	4e	0.509(6)	0.178(7)	0.199(7)	0.034(6)	1.0
O	4e	0.294(4)	0.181(7)	0.279(7)	0.058(6)	0.84(3)

Space group $P2_1/n$, a = 10.591(1) Å, b = 7.525(2) Å, c = 7.318(1) Å, β = 92.24(2)°

Reliability Factors: R_p = 6.04%, R_{wp} = 7.48%, χ^2 = 0.84

Table S3. Structural parameters and atomic positions obtained from Rietveld refinement of PXRD data on MnNi-PBA.

Atom	**site**	**x**	**y**	**z**	U_{iso}	**Occupancy**
Mn/Ni	2a	0.5	0.5	0.5	0.013(3)	0.5/0.5
Fe	2d	0.5	0	1.0	0.044(5)	0.99(2)
Na	4e	0.292(2)	0.460(4)	0.001(4)	0.076(6)	0.99(3)
N	4e	0.497(8)	0.288(8)	0.748(9)	0.031(4)	1.0
N	4e	0.287(4)	0.538(8)	0.518(8)	0.031(4)	1.0
N	4e	0.504(6)	0.318(7)	0.289(8)	0.031(4)	1.0
C	4e	0.479(8)	0.202(8)	0.815(8)	0.031(4)	1.0
C	4e	0.189(4)	0.452(9)	0.530(8)	0.031(4)	1.0
C	4e	0.467(8)	0.182(8)	0.194(9)	0.031(4)	1.0
O	4e	0.246(7)	0.216(6)	0.284(7)	0.034(11)	1.00(4)

Space group $P2_1/n$, a = 10.413(2) Å, b = 7.470(2) Å, c = 7.253(3) Å, β = 91.13(2)^o

Reliability Factors: R_p = 3.13%, R_{wp} = 3.99%, χ^2 = 0.79

Supporting Figures

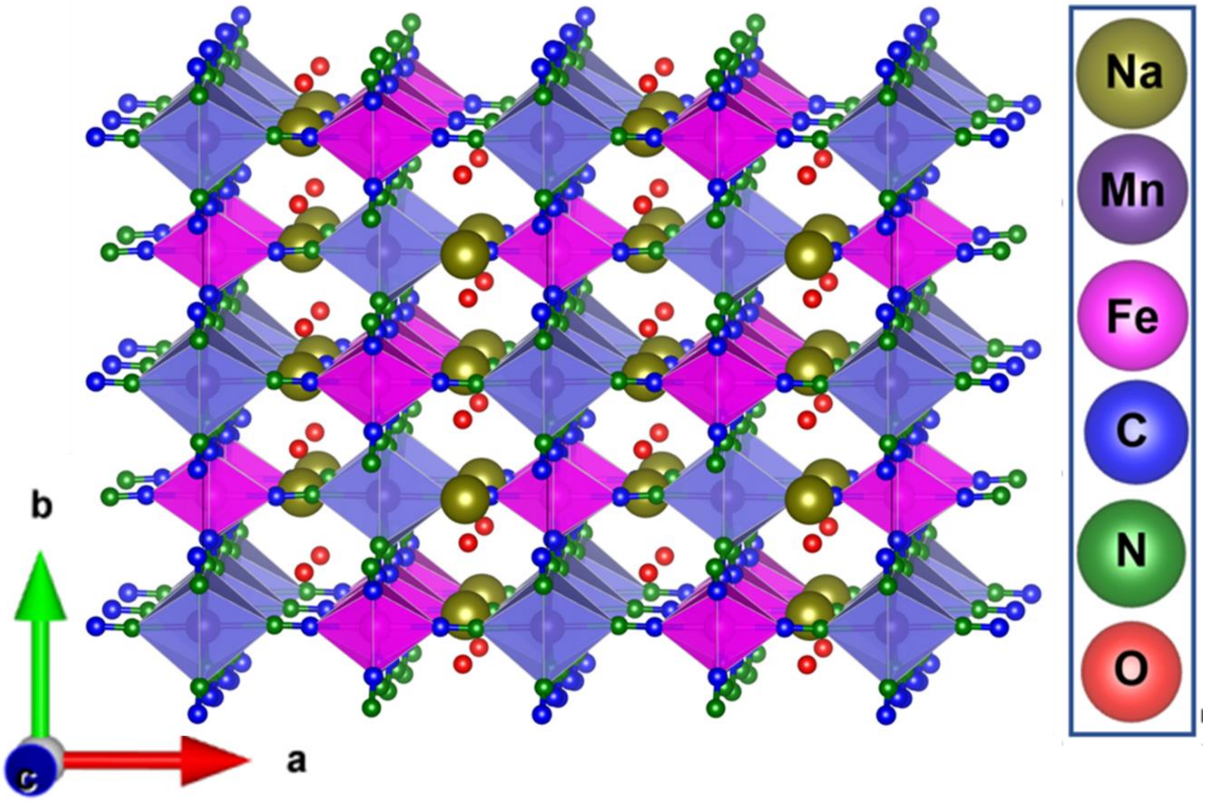

Fig. S1: Crystal structure of Mn-PBA in monoclinic phase (viewed along the crystallographic c direction).

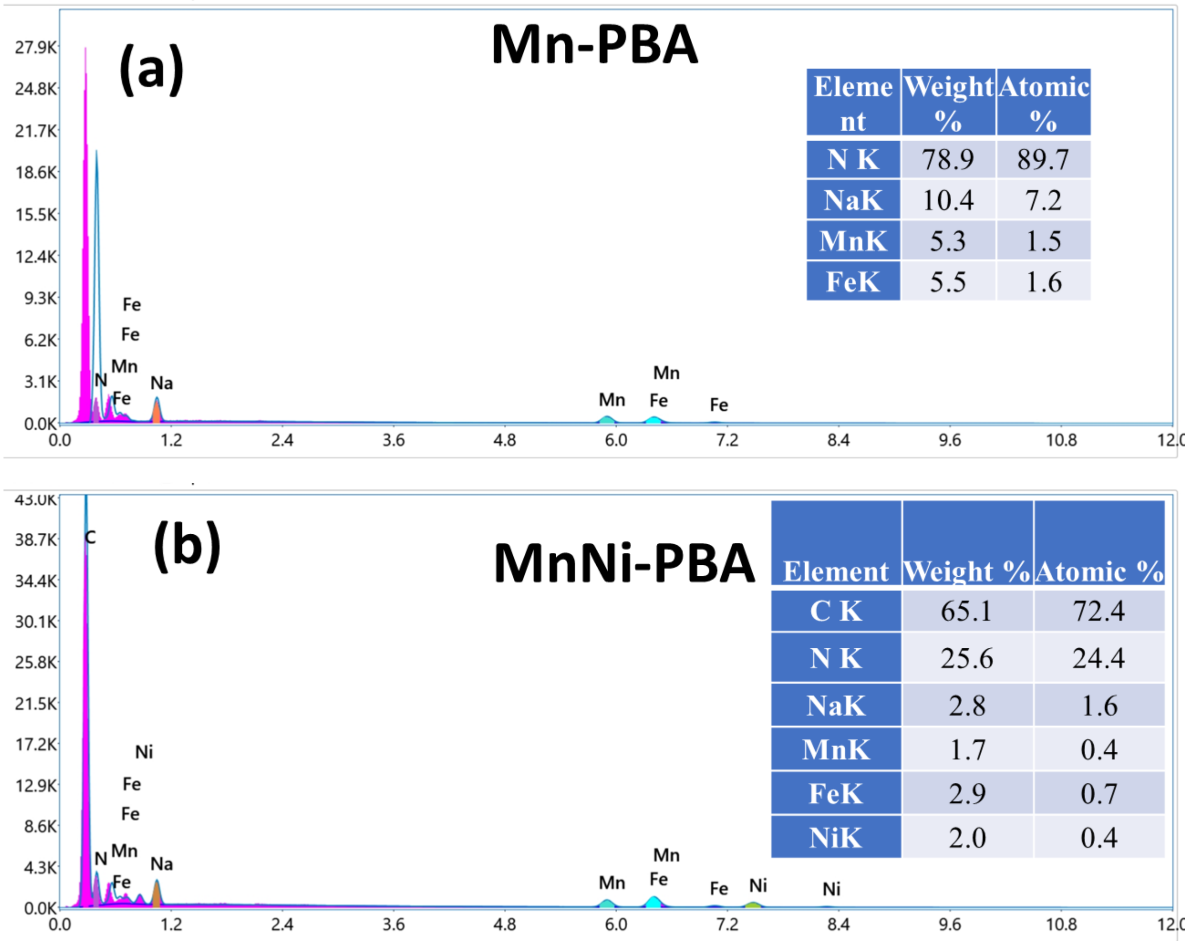

Element	Weight %	Atomic %
N K	78.9	89.7
NaK	10.4	7.2
MnK	5.3	1.5
FeK	5.5	1.6

Element	Weight %	Atomic %
C K	65.1	72.4
N K	25.6	24.4
NaK	2.8	1.6
MnK	1.7	0.4
FeK	2.9	0.7
NiK	2.0	0.4

Fig. S2: EDX analysis of (a) Mn-PBA and (b) MnNi-PBA.

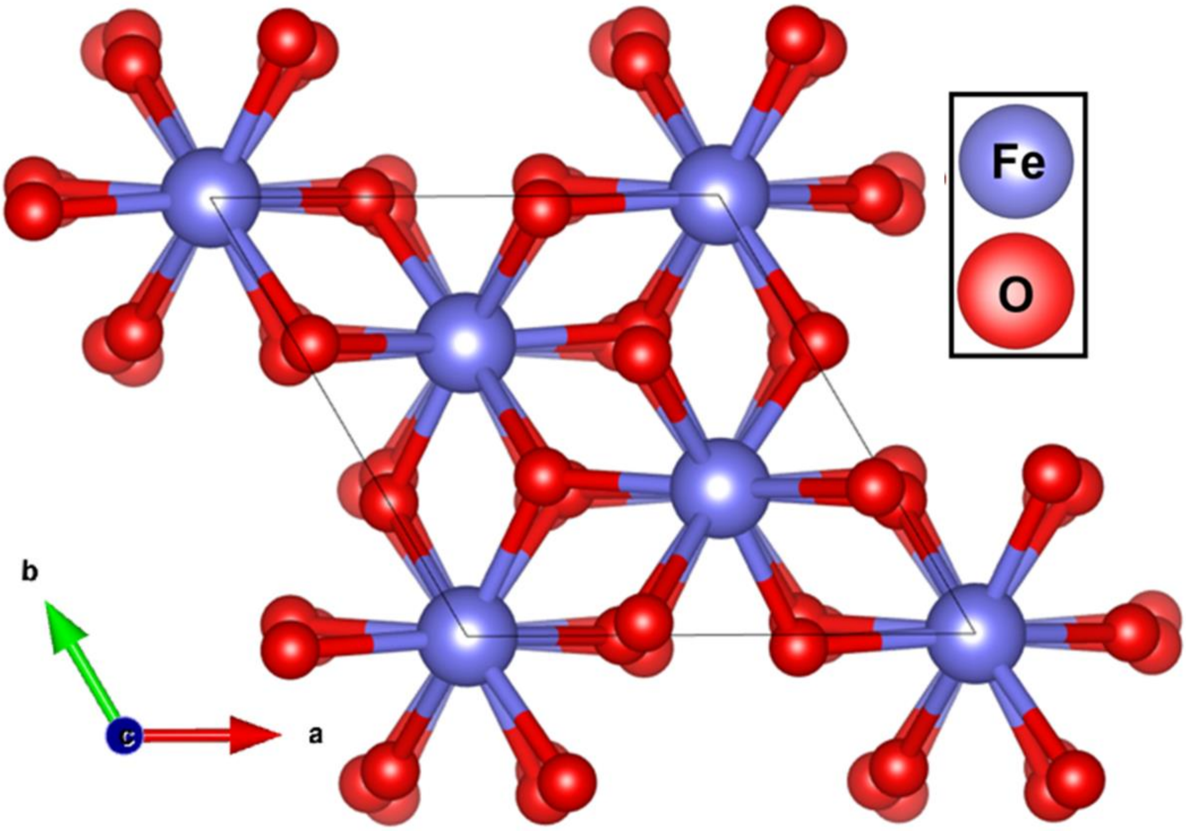

Fig. S3: Crystal structure of Fe_2O_3 in rhombohedral phase (viewed along the crystallographic c direction).

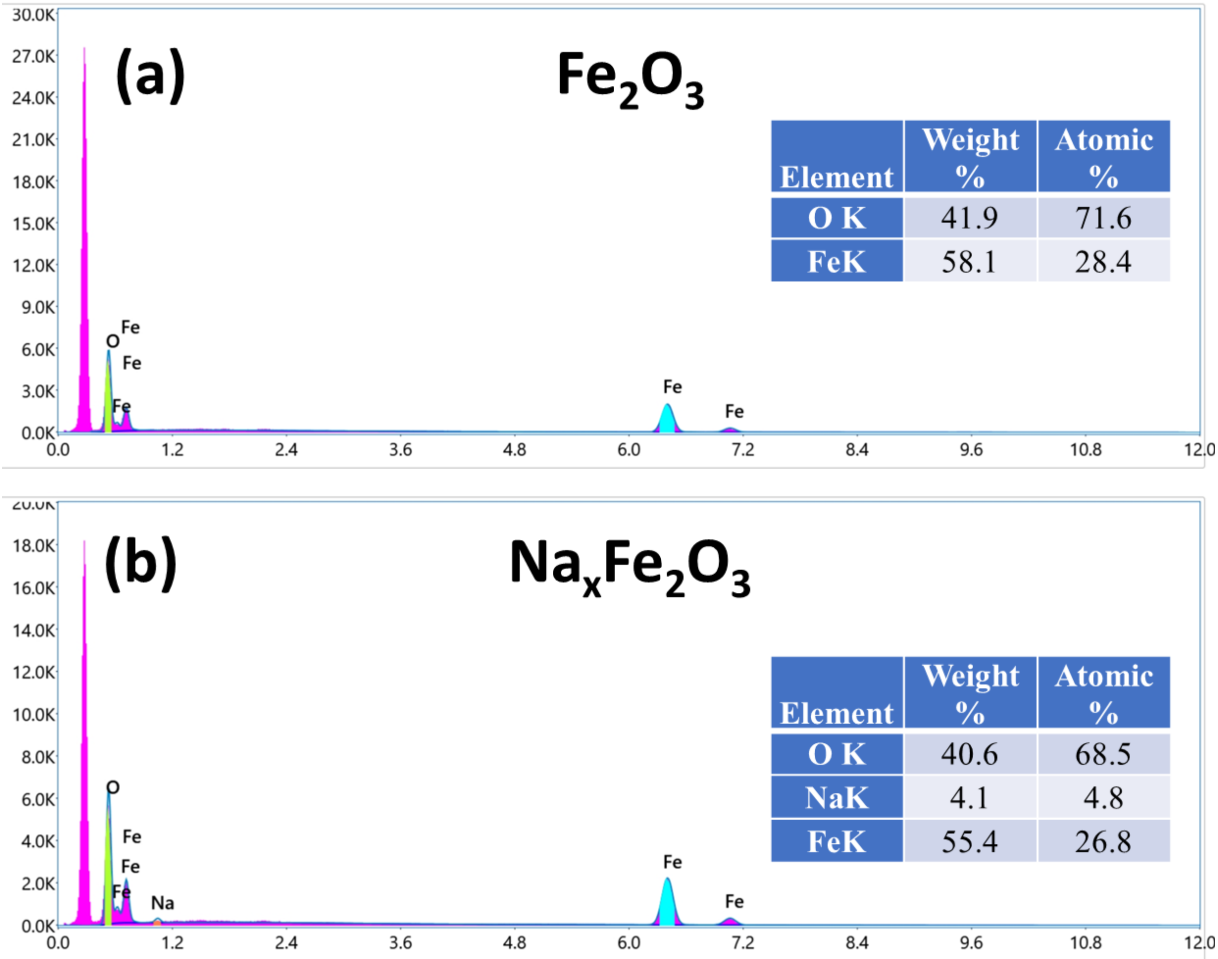

Fig. S4: EDX analysis of (a) Fe_2O_3 and (b) $Na_xFe_2O_3$.

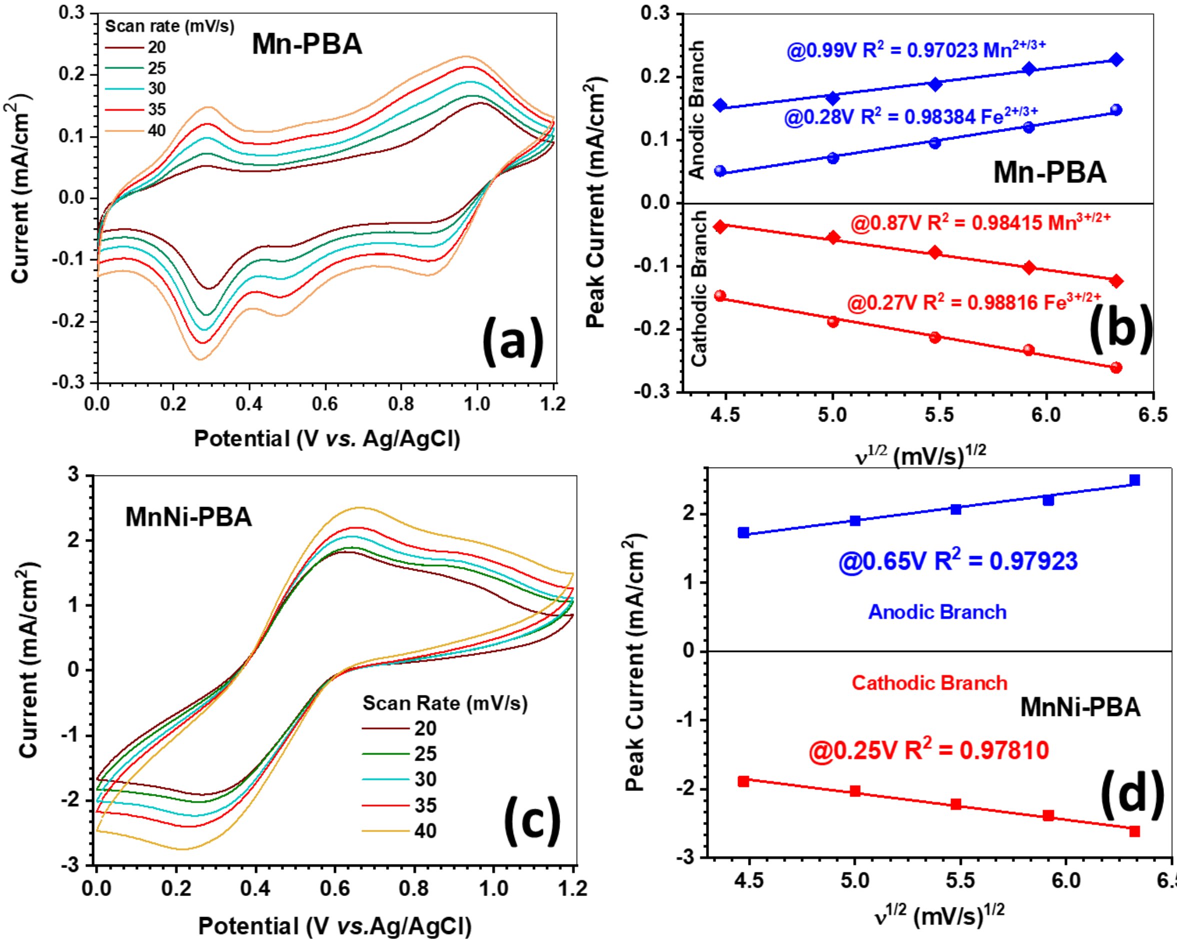

Fig. S5: (a) CV profiles of Mn-PBA at variable scan rates, (b) peak current *vs*. square root of scan rate profiles of Mn-PBA, (c) CV profiles of MnNi-PBA at variable scan rates, (d) peak current *vs*. square root of scan rate profiles of MnNi-PBA.

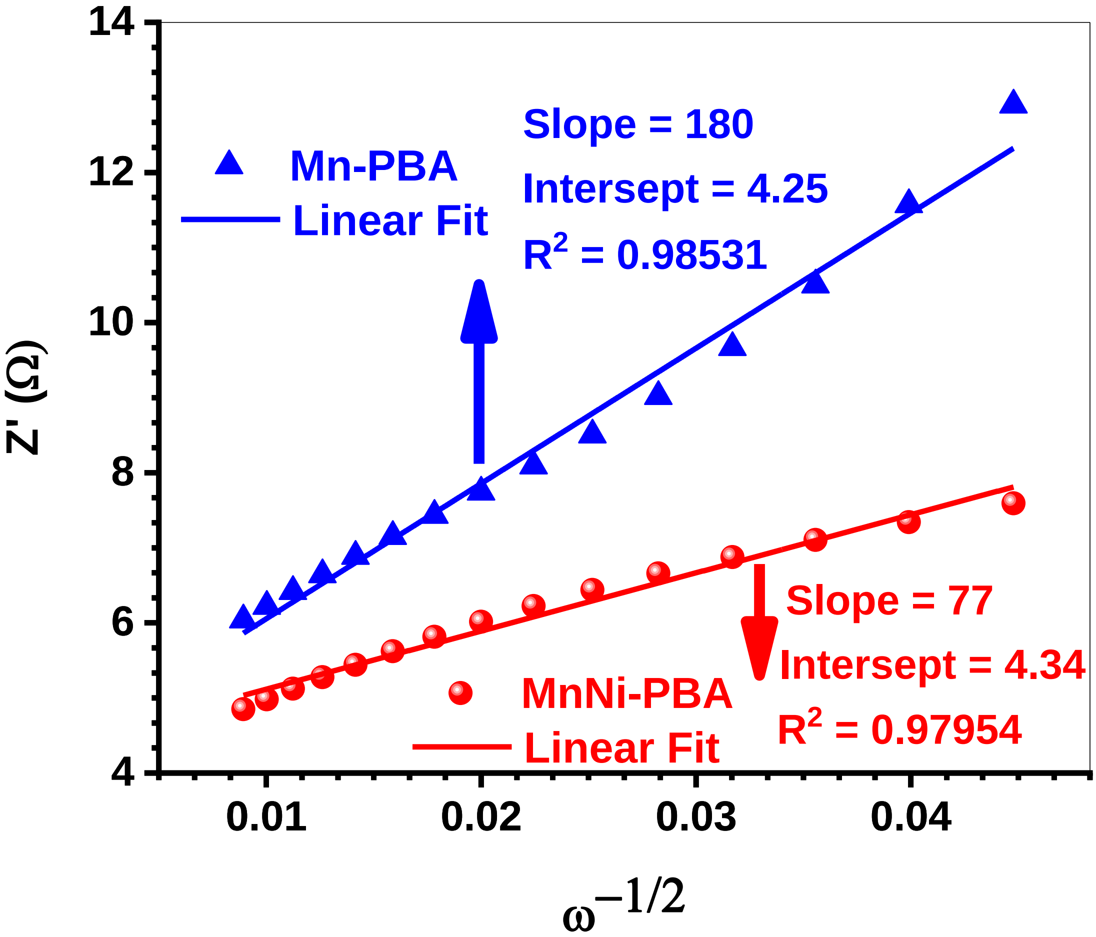

Fig. S6: linear relationship between Z′ and $\omega^{-1/2}$ at low-frequency region in EIS (ω = angular frequency) for Mn-PBA and MnNi-PBA.

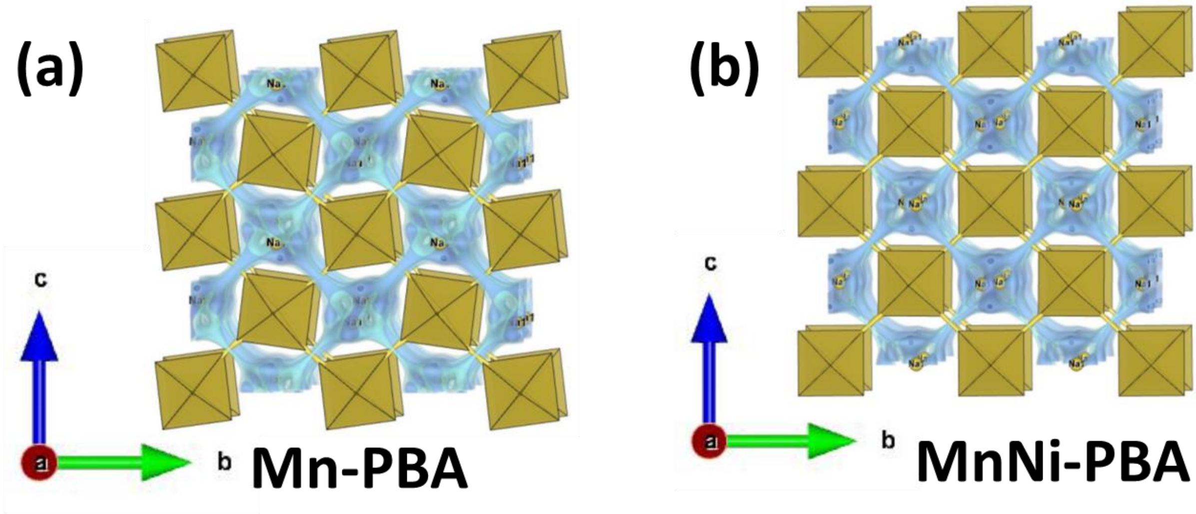

Fig. S7: Na-ion diffusion pathways in the b-c plane as viewed along the crystallographic a-direction: (a) Mn-PBA and (b) MnNi-PBA.

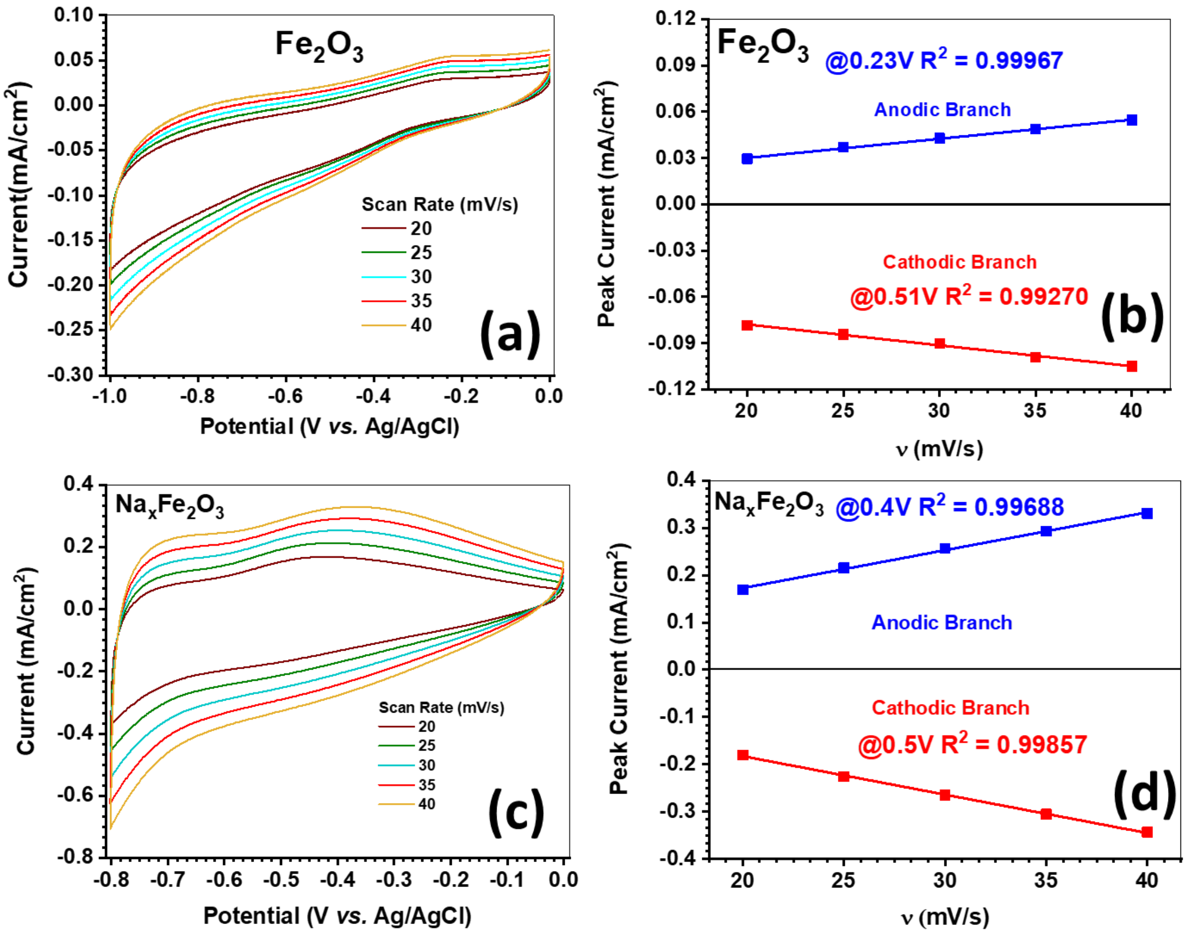

Fig. S8: (a) CV profiles of Fe_2O_3 at variable scan rates, (b) peak current *vs*. scan rate profiles of Fe_2O_3, (c) CV profiles of $Na_xFe_2O_3$ at variable scan rates, (d) peak current *vs*. scan rate profiles of $Na_xFe_2O_3$.

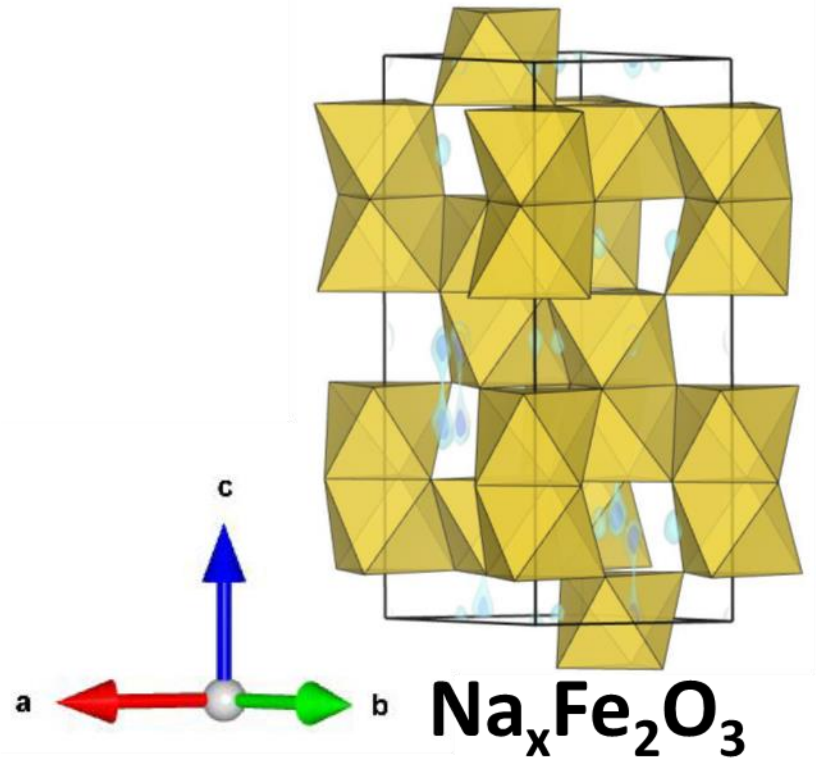

Fig. S9: Na-ion diffusion pathway in $Na_xFe_2O_3$.

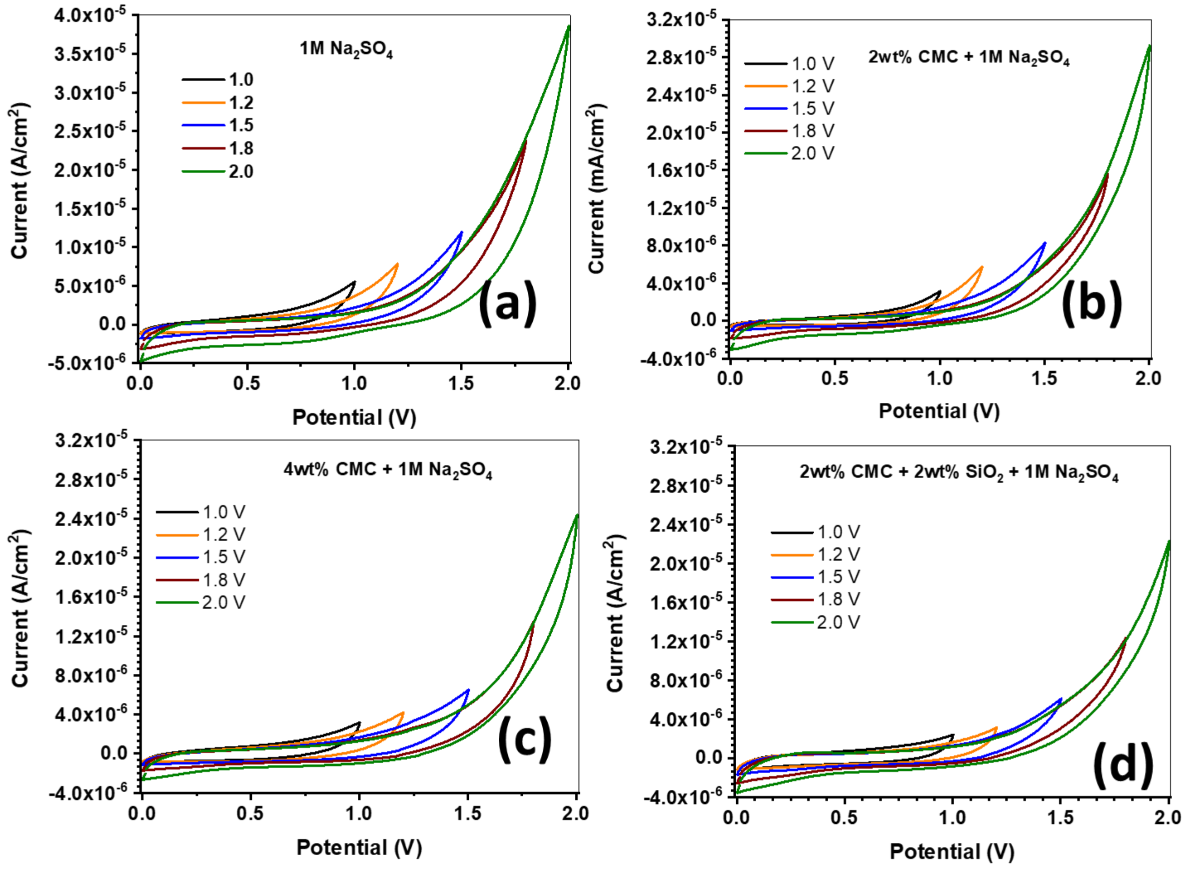

Fig. S10: CV profiles at 10 mV s^{-1} scan rate of symmetric cells with 1 M Na_2SO_4 aqueous electrolyte under (a) flooded, (b) 2 wt% CMC gel, (c) 4 wt% CMC gel and (d) 2 wt% CMC + 2 wt% SiO_2 hybrid gel mediums.

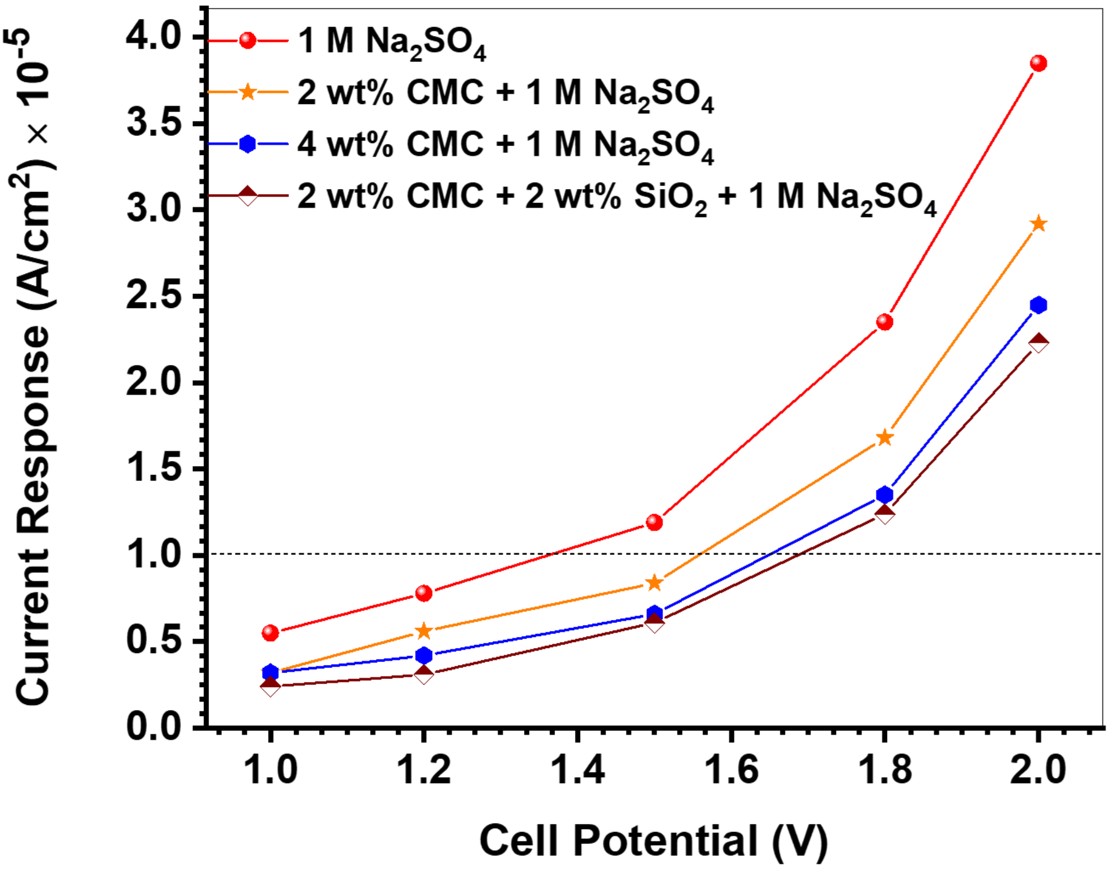

Fig. S11: Current response at various cell potentials of symmetric cells with various electrolyte mediums. Data recorder for this figure from Fig. S8.

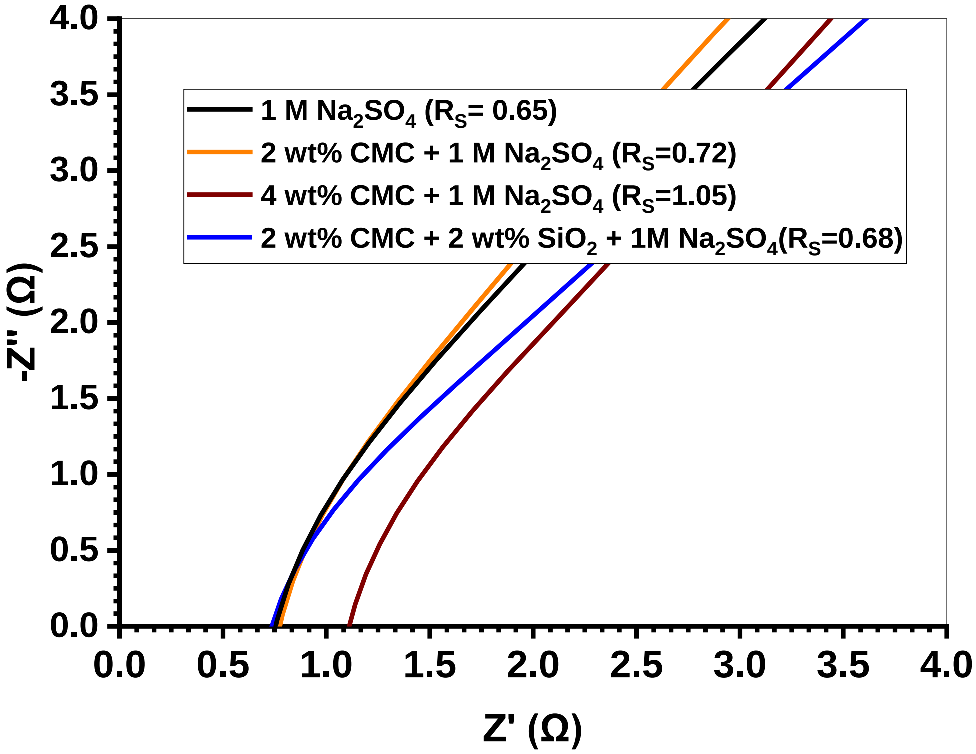

Fig. S12: Nyquist plots of the symmetric cells with various electrolyte mediums.